NAWCWPNS TP 8346

PROPELLANT CONTAINMENT VIA THERMOTROPIC LIQUID CRYSTAL POLYMERS

by

J. J. Rusek
Airframe, Ordnance, and Propulsion Division

and

M. Macler
Laser Consultant

MARCH 1998

NAVAL AIR WARFARE CENTER WEAPONS DIVISION
CHINA LAKE, CA 93555-6100

Approved for public release; distribution is unlimited.

Naval Air Warfare Center Weapons Division

FOREWORD

This report presents an investigation to determine the viability of a development program targeted at developing a storable propellant container by using liquid crystal polymer technology. Different processing and joining techniques are explored, and their advantages and disadvantages evaluated.

This effort was supported by the Ballistic Missile Defense Office and managed by Mr. Ken Hampsten, Phillips Laboratory, Kirtland Air Force Base.

This report has been reviewed for technical accuracy by Stuart Blashill.

Approved by
J. ROBBINS, *Head*
Airframe, Ordnance, and Propulsion Division
30 March 1998

Under authority of
RAND H. FISHER
RADM, U.S. Navy
Commander

Released for publication by
S. HAALAND
Director for Research and Engineering

NAWCWPNS Technical Publication 8346

Published by ..... Technical Information Division
Collation ..... Cover, 28 leaves
First printing ..... 90 copies

REPORT DOCUMENTATION PAGE

Form Approved OMB No. 0704-0188

1. AGENCY USE ONLY (Leave blank)	2. REPORT DATE	3. REPORT TYPE AND DATES COVERED
	March 1998	Summary

4. TITLE AND SUBTITLE

PROPELLANT CONTAINMENT VIA THERMOTROPIC LIQUID CRYSTAL POLYMERS

5. FUNDING NUMBERS

6. AUTHOR(S)

J. J. Rusek and M. Macler

7. PERFORMING ORGANIZATION NAME(S) AND ADDRESS(ES)

Naval Air Warfare Center Weapons Division
1 Administration Circle
China Lake, CA 93555-6100

8. PERFORMING ORGANIZATION REPORT NUMBER

NAWCWPNS TP 8346

8. SPONSORING/MONITORING AGENCY NAME(S) AND ADDRESS(ES)

Ballistic Missile Defense Office
Washington, DC

10. SPONSORING/MONITORING AGENCY REPORT NUMBER

11. SUPPLEMENTARY NOTES

12a. DISTRIBUTION/AVAILABILITY STATEMENT

A statement; approved for public release; distribution is unlimited.

12b. DISTRIBUTION CODE

13. ABSTRACT (Maximum 200 words)

(U) This report presents an investigation to determine the viability of a program targeted at developing a storable propellant container by using liquid crystal polymer technology. Different processing and joining techniques are explored, and their advantages and disadvantages are evaluated.

14. SUBJECT TERMS

Liquid Crystal Polymers, Thermoforming Processing, Injection Molding, Stretch Blow Molding, Extrusion Blow Molding, Joining Techniques, Mechanical Fastening, Adhesive Bonding, Solvent Bonding, Welding, Laser Welding

15. NUMBER OF PAGES

54

16. PRICE CODE

17. SECURITY CLASSIFICATION OF REPORT	18. SECURITY CLASSIFICATION OF THIS PAGE	19. SECURITY CLASSIFICATION OF ABSTRACT	20. LIMITATION OF ABSTRACT
UNCLASSIFIED	UNCLASSIFIED	UNCLASSIFIED	SAR

CONTENTS

ACKNOWLEDGMENTS

The authors would like to thank Mr. Ashley Sabin of Hoechst Celanese Corporation for all his help in acquiring resin properties and for his production insight; Mr. Chris Frank of the Advanced Composites Program Office at McClellan Air Force Base for the continued dialogue on polymer processing; and Ms. Angelia Weeks of the McClellan Nuclear Reactor Center for nuclear testing and insight into impurity determination of polymers.

The authors also wish to gratefully acknowledge the funding received from the Ballistic Missile Defense Office. Mr. Ken Hampsten, Phillips Laboratory, Kirtland Air Force Base, was the program manager. The U.S. Air Force deserves praise for not only funding this effort, but also for having the foresight to explore new materials and new propulsion concepts which will allow mankind to come ever closer to the stars.

INTRODUCTION

The Ballistic Missile Defense Organization, formerly known as the Strategic Defense Initiative Organization, is currently supporting the Space Based Laser (SBL) program. The SBL offers benefits in countering a generalized ballistic missile threat. The proposed concept consists of orbiting twenty SBLs in a defined constellation, which, in concert with other Theater Ballistic Missile Defense options, have the capability of mitigating offensive ballistic missile threats. In order to effect the constellation, novel technologies must be explored to ensure the timely development, manufacture, and deployment of these innovative defensive weapons.

The SBL uses a fluorine-based chemical laser as its primary device; it is planned to be lofted to orbit by a set of liquid oxygen-kerosene engine stages. The propellants will be likely pressure-fed by a liquid-based gas generator comprised of the 'monopropellant' hydroxylammonium nitrate/triethanolamine/ water. It is essential that inert weight (tankage) be kept to an absolute minimum while ensuring adequate reliability and low cost. At first, these parameters appear to be at odds with one another, but technology has progressed in a direction where they are not mutually exclusive.

Project Scorpius was initiated to prove the feasibility of an inexpensive launch vehicle concept to loft the SBL system. The objective of this document is to expand on near-term practical solutions to the seeming paradox cited above. The key to solving the problem lies in the use of advanced polymeric materials.

TECHNICAL CONCEPT

It is envisioned that low-cost, lightweight tanks be fabricated of thermotropic liquid crystal polymers (tLCPs) using novel fabrication techniques to ensure light weight and high strength. The tLCPs have demonstrated high strengths, low permeation rates, chemical compatibility, and amenability to a variety of innovative processing and joining technologies.

The processing techniques to be used are advanced injection molding and blow molding. Novel joining techniques that utilize real-time laser radiation impingement coupled with both convolute- and filament-winding techniques are also envisioned.

The tanks fabricated with tLCPs will be used as gas generator liquid storage tanks, propellant tanks, and, potentially, even as flightweight lasing fluid tanks. This technology has the added benefit of being applicable, and therefore transferable, to the automotive, maritime, and chemical communities.

LIQUID CRYSTAL POLYMERS

The advent of advanced composite materials has led to aerospace articles with high specific strength and modulus. A significant drawback to these components is their long fabrication time, lack of consistency, and high cost. In contrast, articles produced from commodity thermoplastics yield reproducible, low cost items with very low specific strengths. The discovery of thermotropic liquid crystal polymers over thirty years ago promised articles with the best properties of both—high reproducibility, lower cost, and high performance.

Thermotropic liquid crystal polymers are true hybrids of the advanced composites and commodity thermoplastics technologies. They are the strongest engineering thermoplastics available for commercial use. Their low weight, chemical resistance, and ease of processing make them logical candidates for astronautics applications. The fact that these materials are liquid crystalline in nature and can be quenched to form a molecular composite is both a benefit and a liability. The thermal processing and post-processing become the prime determinant of the ultimate properties of the component.

Liquid crystalline materials have been known for over one hundred years. The tobacco mosaic virus and isolated cholesterol were noted to exhibit liquid crystalline behavior in solution. The last thirty years have heralded liquid crystalline polymers—species that exhibit liquid crystalline behavior in solution (lyotropes) and a new class of materials that exhibits this behavior in the molten state (thermotropes). The commercial grades of these species are well known as the strongest thermoplastics in existence, have excellent chemical and thermal resistance, and are lightweight.

Three liquid crystalline states have been identified: nematic, smectic, and cholesteric. These states are shown in Figure 1. An increase in molecular order occurs from nematic to smectic to cholesteric; however, potential fracture planes become more evident. For structural applications, the nematic phase is the preferred orientation.

Polymeric lyotropes, such as KEVLAR, form from a highly acidic solution. The lyotropes exhibit a nematic crystalline phase but can only be drawn into fibers or, at best, thin sheets. Polymeric thermotropes such as VECTRA, XYDAR, and ZENITE form nematic phases in the melt that can be retained via quenching to yield a highly oriented, macroscopic part.

Researchers at Phillips Laboratory, Edwards Air Force Base, Calif., have been actively pursuing thermally processed liquid crystal polymers for the past six years under an in-house initiative called Advanced Polymer Components (References 1-3). The tables of contents of the publications addressing this topic are included in Appendix A. The targeted application area is structural propulsion components. All propulsion system requirements demand high performance coupled with low weight and cost. The advent of a variety of commercial liquid crystalline materials makes the timing ideal for component application.

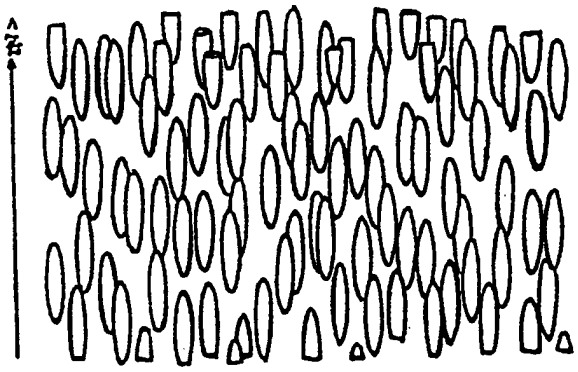

(a) Nematic Phase.

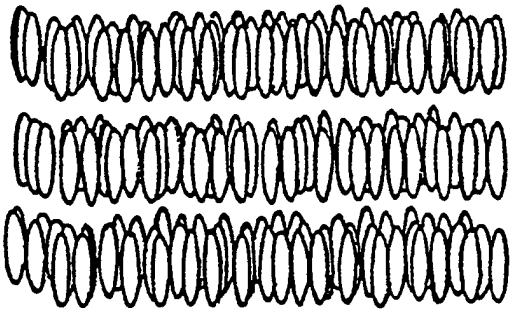

(b) Smectic Phase.

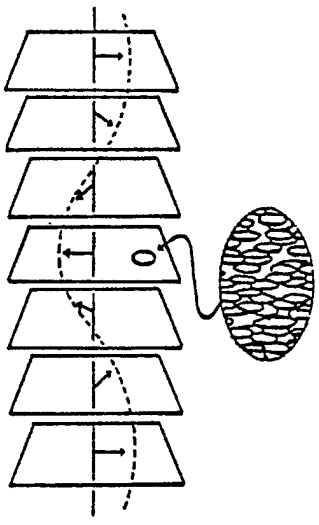

(c) Cholesteric Phase.

FIGURE 1. Representation of Liquid Crystalline Behavior.

Initially, commercial thermotropic resins were molded and tested as propulsion test articles (References 1-3). The physical properties of the skin region were found to be quite different from those of the interior core. Sectioned specimens were analyzed and found to be different not only in strength but also in chemical and thermal properties. Post-thermal processing (annealing) of the liquid crystalline materials gave as much as a twofold increase in tensile strength for certain polymers (ZENITE precursors). This led to a significant fundamental research component directed toward understanding the annealing phenomenon.

The annealing phenomenon manifested itself as an increased resistance to chemical attack and a dramatic increase or obviation of the traditional polymer melt temperature. Past work has indicated that the annealing phenomenon does not involve cross-linking or traditional chain-extension as noted in other polymeric systems (References 1-3).

The work accomplished under the Advanced Polymer Components Initiative has led to the following conclusions:

1) Liquid crystal polymers have a viable role in rocket propulsion as advanced ablative, pressure containment, and cryogenic storage materials.

2) The polymer strengths can be increased further by annealing.

3) The chemical resistance of these polymers is excellent, with little degradation in properties by contact with most solvents.

4) Chemical resistance with respect to monomethylhydrazine and nitrogen tetroxide can be improved by annealing; however, traditional storable propellant containment is not recommended.

5) The mechanical properties remain the same, or improve, with a decrease in temperature, down through liquid hydrogen temperatures. These polymeric materials also have low permeability; hence, liquid hydrogen containment is recommended.

6) Reactivity with liquid oxygen is within a factor of three relative to TEFLON, a material classed for oxygen service. Specific applications for liquid oxygen containment should be explored.

7) Completely plastic solid rocket motors have been fired successfully. Ablation rates and pressure values have established that the liquid crystalline materials are good candidates for tactical applications.

8) Thermotropic liquid crystal polymers have higher strengths in the skin region; thin extruded or blow-molded components have higher specific tensile strengths than thicker injection-molded components.

It is clear that thermotropic liquid crystal polymers have a significant role in solid and liquid propulsion. The advent of advanced propulsion concepts, such as hybrid propulsion with non-toxic storable oxidizers, demands extreme materials properties for successful accomplishment. Thermotropic liquid crystal polymers are excellent candidates for these future systems.

Liquid crystal polymers promise rocket propulsion systems that are responsive, flexible, and low cost, both in the space-lift and the tactical arenas. These materials, when coupled with advanced propulsion concepts, should enable the next-generation of aerospace vehicles, from tactical (Reference 4), through strategic, and leading to next-generation transatmospheric vehicles.

THERMOFORMING PROCESSING TECHNIQUES

INJECTION MOLDING

The most widely used type of thermoforming operation (Reference 5) for plastic materials is that of injection molding. Injection molding is a manufacturing process which capitalizes on high production rates. In general, the type of polymer used in this process is thermoplastic, meaning that it can be reformed by the application of heat. The two key pieces of equipment required are the mold, or die, and the injection-molding machine. The machine heats the plastic to its melting point by electrical and mechanical (shear) heating, this is done in the injection unit with a rotating screw located inside the barrel. The machine then forces the molten plastic into the mold using the screw as a ram, in a second operation. A generalized injection-molding machine is shown in Figure 2.

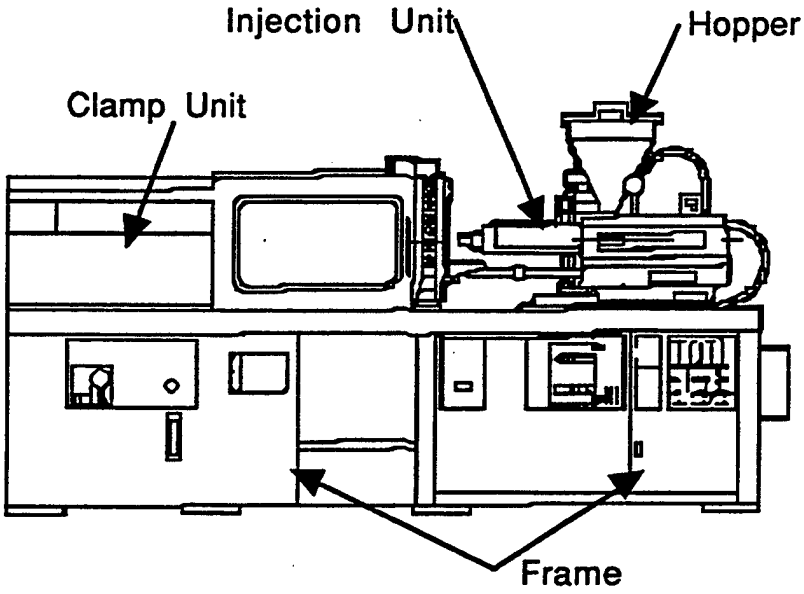

FIGURE 2. Generalized Diagram of an Injection-Molding Machine.

The applied force is sometimes very high (as much as 20,000 psi); therefore, a large clamping force is required to keep the mold from opening or deforming while the plastic is being forced into the mold cavity. The clamp section of the machine is designed to maintain uniform pressure on the mold to keep it closed and in place.

After the plastic is injected into the mold, the clamping force keeps the mold closed until the plastic cools. The mold is then opened, and the molded parts are removed by hand or by a mechanical ejection system. This happens each time a part is molded.

The mold that defines the part, usually made of steel, must retain its shape while being subjected to extreme pressures and temperatures. The mold is a nearly solid block of metal. The center of the mold is a cavity, which defines the shape of the part. The tool must withstand hundreds to thousands of clamping cycles, with commensurate heating and cooling, during which it must maintain all of its accurate dimensions.

Using this process, very intricate parts can be made, as thin as 0.010 inch and with a high degree of detail. What really controls the intricacy of the part is the mold; thus, the more detailed the part, the more detailed the tool, and the more expensive it becomes. If the number of parts to be molded is small, aluminum can be used, but if a large number of parts are required, or the tool has sliding details or actions, then steel is the only choice.

The most striking advantages of injection molding are its repeatability over a large number of parts and the detail that can be included in the primary process of molding. A good deal of detail, such as tabs, holes, and threads, can be defined by molding, thereby reducing the amount of post-processing required. Moreover, after the tooling is paid for, the cost per part for manufacturing remains relatively low. Molds can be of three styles: manual, semi-automatic, and automatic. The factors in determining style are quantity and cost. Manual dies usually consist of a single cavity and are put together and removed by hand. This is a time-consuming operation, because the mold has to be assembled and disassembled by hand while the parts are cooling in the die. These dies are best suited for very short runs of less than 25 parts and, typically, they would run on a small prototyping machine. Semi-automatic dies are more cost effective because they require less manual operation, and parts production is faster. These dies require an ejection system with a sprue puller and are more expensive to build because of the combined mechanical operations involved. These dies are best suited to mid-range runs of more than 100 parts and up to thousands. Automatic dies are the most expensive to build. These dies require ejection, sprue pulling, runner systems, heating and/or cooling systems, and usually more than one cavity.

STRETCH BLOW MOLDING

A second thermoforming process that is of interest is stretch blow molding (Figure 3). In this process, a preform (parison) is injection molded, usually in the form of a test tube shape. The preform is then heated and blown to shape inside a larger tool stretching the tube like a balloon, thus producing the stretch in the hoop direction. The stretch ratio is usually around 4.5 to 1. This process is currently used to produce 1- and 2-liter soda bottles out of poltethylene terephthalate. Using tLCPs, it is envisioned that this process could produce pressure vessels for propellant or gaseous storage.

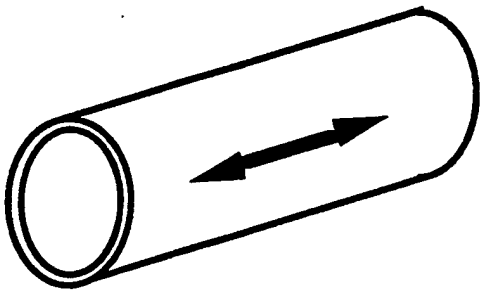

(a) Injection Molded Preform.

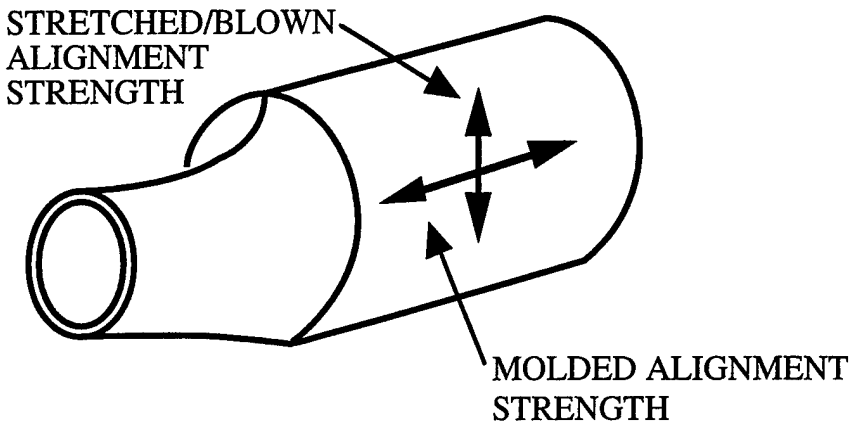

(b) Blown Injection Molded Preform.

FIGURE 3. A Longitudinally Oriented Injection Molded Preform (a) Blown to Increase Hoop Strength (b).

EXTRUSION BLOW MOLDING

A third avenue, via thermoforming, is to use extrusion blow molding. As compared to the stretch blow molding process, which uses two discrete steps, the extrusion process is semi-continuous. The resin is fed to an extruder, and a cylindrical geometry parison is extruded. The extrusion is stopped, the parison clamped, and compressed air admitted to the mold cavity. This process has the benefit of eliminating the parison reheat step, which is significant due to the inherent insulating properties of tLCPs. Investigators of Hoechst Celanese Corporation ran a number of prototype buoys in 1991 to test the value of their VECTRA resin in blow-molding applications to generate high strength components. Using a VECTRA A115 resin, they blow molded several 6-liter tanks, which weighed roughly 1.25 pounds each. Figures 4, 5, and 6 depict the 6-liter pressure bottle that was fabricated by blow molding. Only a few bottles were fabricated, but this certainly points the way to future experimentation.

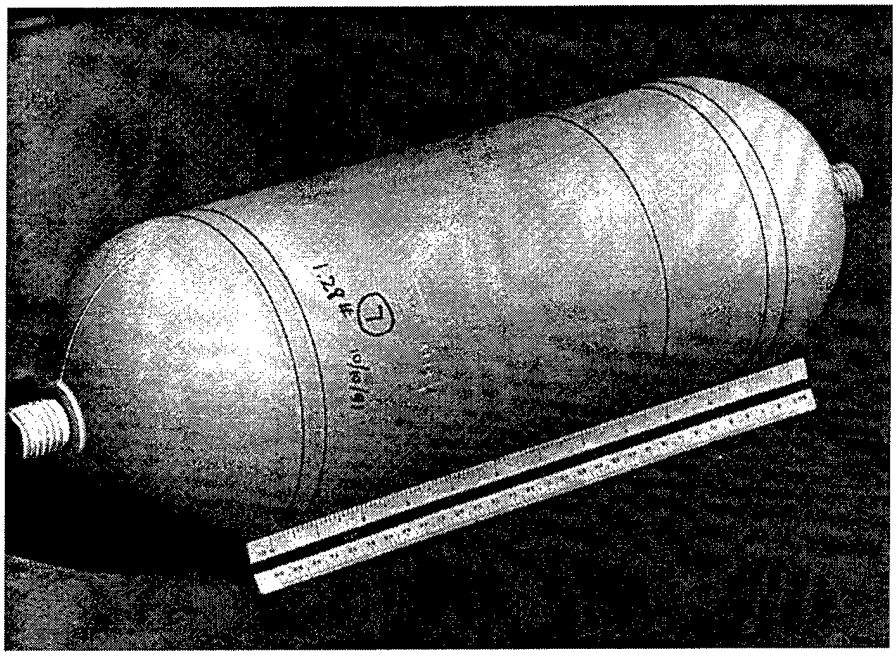

FIGURE 4. View 1 of 6-Liter Blow-Molded Thermotropic Liquid Crystal Polymer Pressure Vessel—VECTRA-Based Resin.

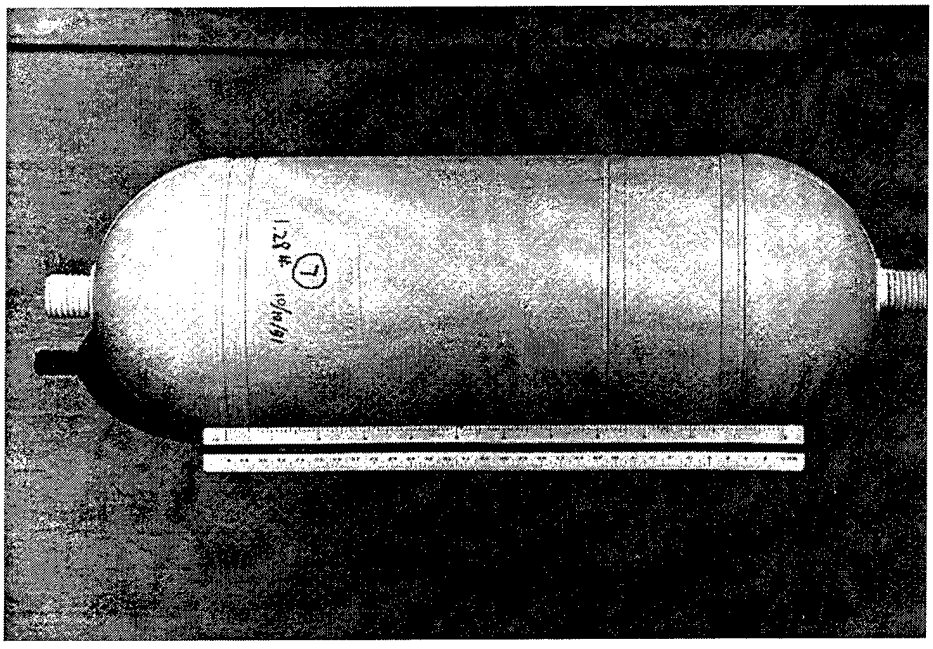

FIGURE 5. View 2 of 6-Liter Blow-Molded Thermotropic Liquid Crystal Polymer Pressure Vessel—VECTRA-Based Resin.

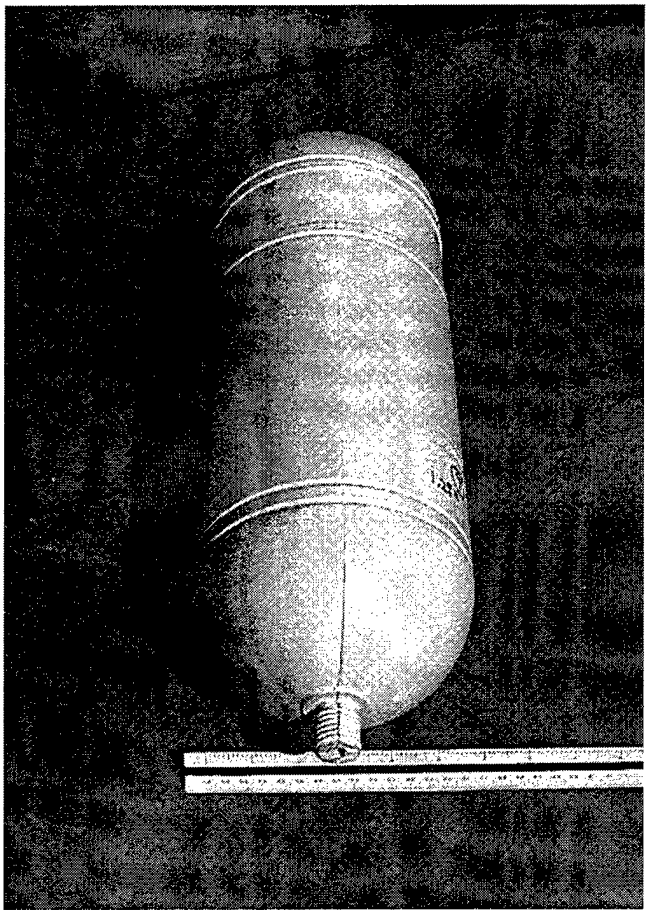

FIGURE 6. View 3 of 6-Liter Blow-Molded Thermotropic Liquid Crystal Polymer Pressure Vessel—VECTRA-Based Resin.

JOINING TECHNIQUES

Joining of thermoplastic parts is becoming increasingly necessary, as thermoplastics are used as load-bearing components in mechanical structures. Yet, little is known about joining thermoplastics. In particular, some forms of welding used on production lines are not well understood. Some are even difficult to control. Serious improvements in joining technologies are necessary if thermoplastics are to realize their potential in load-bearing applications.

Conventional joining techniques are reviewed herein from the standpoint of mass production. Emphasis is placed on feasibility, controllability, cost, and speed. The applicability of these techniques to the joining of VECTRA parts is considered.

Laser welding, while still in the experimental stage, seems to be a technique worth investigating. It is suggested that its application to VECTRA could solve the long-standing problem of liquid crystal polymer joining. A plan to implement this approach is suggested.

CONVENTIONAL JOINING METHODS

Mechanical Fastening

Mechanical fastening is a typical technique for joining VECTRA-based components (References 1-3); however, it is unsuitable for pressure vessels, due to leakage considerations.

Adhesive Bonding

Adhesive bonding was successfully used for VECTRA lap joints in pressure vessels; however, it seems to be limited to a pressure of about 250 psi, which is not high enough for the application discussed herein. Moreover, epoxy glue may not be chemically suitable for use in propellant environments.

Solvent Bonding

Solvent bonding is typically slow, uses generally exotic solvents, and, therefore, is not suitable for mass production.

Welding

Thermal Bonding

Hot gas/extrusion welding is a slow process, considering the insulating properties of the tLCPs; it is difficult to control, and, therefore, not applicable to mass production.

Hot-tool welding is applicable to complex joint geometries, but often a polytetrafluoroethylene (PTFE) coating of the hot metal part is needed to prevent sticking. The operating temperature is limited to 500°F (260°C). This temperature is too low to melt VECTRA. In addition, the relationship between weld parameters and joint strength are not understood.

In summary, thermal bonding is too slow and not controlled well enough for mass production.

Friction Welding

Spin welding is fast and simple and it is used to bond circular cross sections. However, the mechanism by which bonding occurs is not well understood.

Vibration welding is limited to flat seams. It requires simple equipment and is insensitive to surface preparation. It is very controllable. Material degrading due to overheating is unlikely; moreover, cycle times are short.

Ultrasonic welding is limited to small joints. The design of the joint itself needs to be well thought out for ultrasonic welding. It is typically automated and requires compact equipment. Again, cycle time is short.

Overall, friction welding is fast and controllable, but different kinds of joints require the development of different techniques.

Electromagnetic Bonding

Resistance (implant) welding is simple and applicable to complex joint geometries. Weld times are short; however, the implant left in the joint may affect its strength. It is relatively expensive because each joint requires a new implant.

Electrofusion uses a sleeve instead of an implant. Typically, its use is limited to small diameter pipes. It is also relatively expensive.

Induction welding is suitable for very complex joint geometries. The joint can be opened by induction reheating of the implant. However, the implant may affect the joint adversely. It is relatively expensive.

Dielectric welding is used with materials with a high dielectric loss factor. It is usually used for films and thin sheets. It is fast but requires significant capital equipment.

Electromagnetic bonding is fast but expensive. Implants may be a problem for joint strength. It is not suitable for mass production.

In summary, none of the conventional joining methods seem suitable for mass production of load-bearing liquid crystalline polymer parts. Friction welding is fast, simple, and inexpensive, but no single technique is flexible enough for welding all types of joints. To minimize development cost, the chosen technique should only require material-specific optimization.

LASER WELDING

Laser welding is still an experimental technique. Unlike friction welding, it is not used on production lines. There have been few reports of thermoplastic welding in the scientific literature.

The laser of choice has been the continuous wave carbon dioxide laser. This laser emits around 10.6 μm where a significant number of polymers absorb. The CO_2 laser output lines are shown in Figure 7.

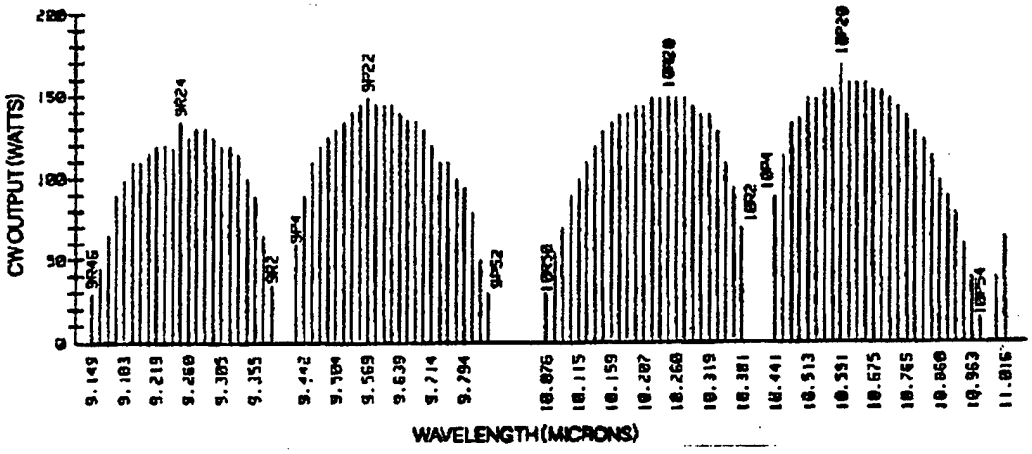

FIGURE 7. Representation of Carbon Dioxide Laser Output Lines.

The features of CO_2 laser welding of polymers can be summarized as follows:

- Good penetration at low laser power.
- Fast processing speeds.
- Small heat-affected zone.
- Fit not too critical.
- Non-contact process.
- Can be used with many polymers.

Successful laser welding of polyethylene was reported as early as 1972 (Reference 6). A 1.5-mm-deep weld was achieved at a speed of 1 cm/s, with a laser power of 100 W. By all accounts, this is fast joining with a low-cost, low-power laser.

In 1992, deep welding of polypropylene was reported (Reference 7). A weld depth of 1.5 cm was achieved at 0.0625 cm/s, with 22 W of laser power. This weld is much slower, but also much deeper than in the case of polyethylene. Higher speeds require higher power, which results in much higher surface temperatures, and possibly degradation of the polymer.

A 1995 publication presented the laser welding of polycarbonate (Reference 8). A 0.45-mm-deep weld was achieved at 0.31 cm/s at a laser power of 8 W, with a duty cycle of 0.018. The depth of this weld may seem small, but it was achieved with only 8 W of laser power. Such a laser, with necessary accessories, costs less than $10,000, is compact (table top), and does not require running water cooling.

No satisfactory theory or model of the welding process exists. Most modeling was conducted for the welding of metals (Appendix B), which behave differently. In particular, the penetration depth of the laser radiation is very small for metals, because the process is governed by conduction. Not surprisingly, all models are based on the heat diffusion equation.

Thermoplastics have much smaller heat conductivities than metals, and the laser radiation penetrates much deeper inside the work piece. Theorists have shown that the laser polymer interaction is very complex (Reference 9). In particular, the infrared absorption spectrum of the polymer changes with temperature. The absorption lines shift toward lower wavelengths as the temperature rises. This effect can be quite pronounced upon melting. The shift is in fact a form of self-regulation of the amount of laser energy absorbed by the work piece. It allows the melted and hottest part of the polymer to become partially transparent, letting the radiation reach the cooler, more absorbing part of the polymer. This phenomenon allows for deep penetration welding, well beyond the laser radiation range given by room-temperature, low-intensity absorption measurements.

The existence of keyholing in polymer welding has been debated (Reference 10). Figure 8 shows a schematic of the keyhole geometry during penetration welding. Those who argued against the keyholing phenomenon have considered the lack of boiling point of most polymers, and their much higher melt viscosities than those of metals. However, some have argued about laser energy losses due to recirculation of the melt in the keyhole (Reference 7). It is the authors' opinion that the latter argument, i.e., the detuning of the absorption spectrum of the work piece, is a better explanation for deep welding than keyholing.

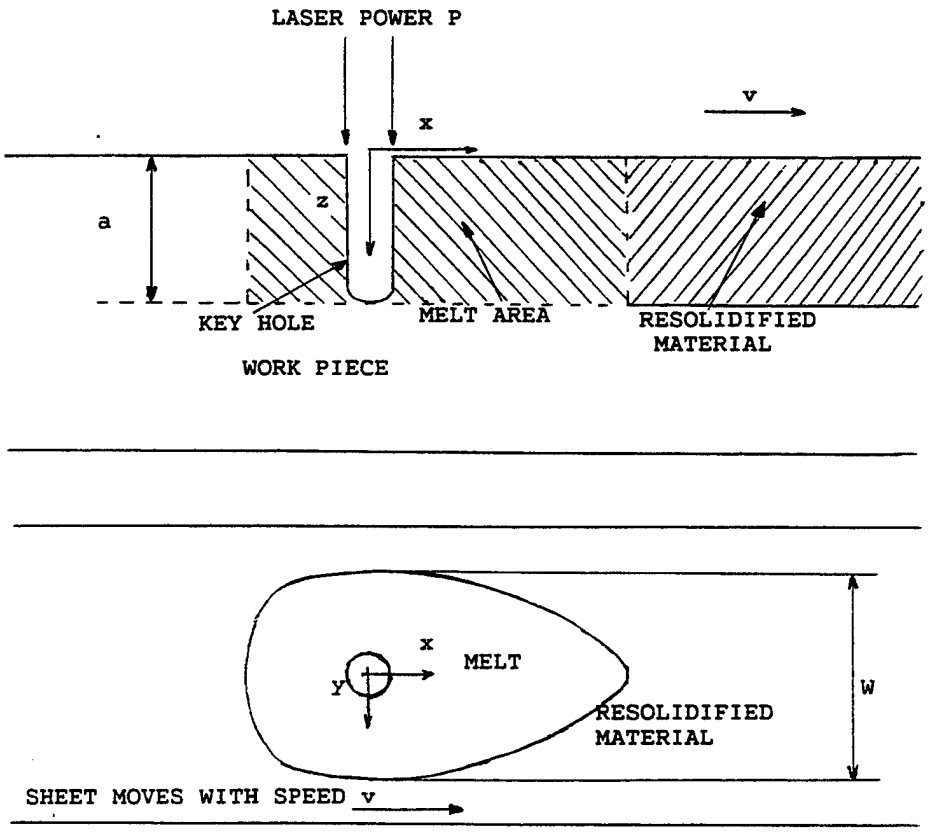

FIGURE 8. Geometry of Keyhole During Laser Penetration Welding.

Polyethylene and polypropylene are considered weak absorbers at the wavelengths of interest. On the other hand, polycarbonate is a strong absorber. The main difference in the experimental results mentioned above is that the speed of welding is higher for weak absorbers. That is because the surface of a strong absorber warms up much faster. Nonlinear effects in the absorption process can degrade the surface and weaken the joint. Therefore, a gradual heating using a chopped laser beam is preferable to continuous exposure. Strong absorbers can be welded in depth, but they require slower welding speed and lower laser power.

It was found experimentally for polypropylene (Reference 7) that

$$P = KvWA \tag{1}$$

where P is the laser power, K is a constant, v is the welding speed, W is the laser beam width, and A is the welding depth. This relationship is very important because it can guide the development of the welding process.

Laser welding of thermoplastics is controllable and fairly inexpensive. It is also flexible and reliable. The laser beam can be delivered to hard-to-reach places and, in most cases, its cycle time is short.

VECTRA is a strong absorber around the CO_2 laser wavelength, because of the presence of C-O bonds in the monomer. An infrared absorption spectrum is shown in Figure 9. It also has a fairly high melting point (280-300°C) and a thermal diffusivity like that of polycarbonate. Therefore, VECTRA is expected to behave like polycarbonate during welding.

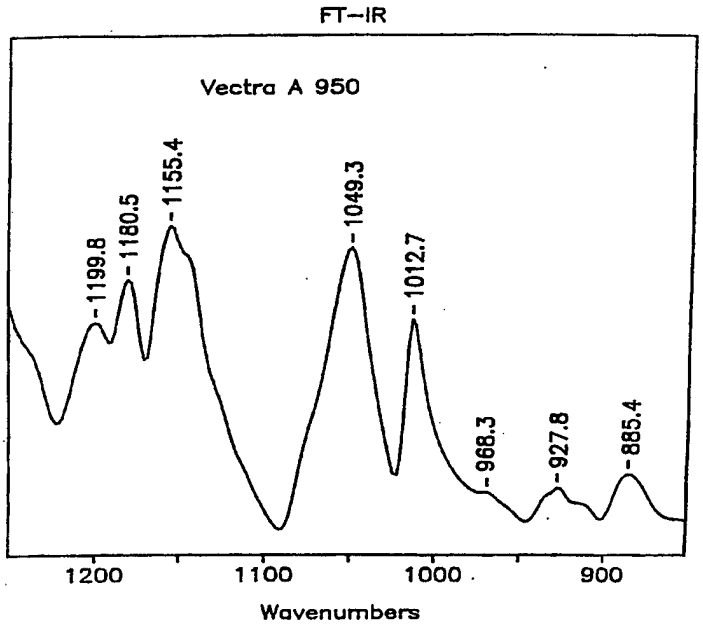

FIGURE 9. Absorption Spectrum of VECTRA A950 Polyester.

VECTRA has a very low melt viscosity, as is expected from liquid crystal polymers, and a high degradation temperature (454°C). These two properties are very valuable for welding depth and speed. The low viscosity can help enhance the welding depth through keyholing. The high degradation temperature should allow for higher duty cycle, and, consequently, faster welding speed.

The authors' approach to welding VECTRA consists in starting with a chopped beam, which will provide a heating scheme similar to that used for welding polycarbonate (i.e., the spinning of the cylinders in front of the laser beam) (Reference 8). Pulsed heating will be used to prevent the degradation of the surface, while retaining a decent weld depth. The actual duty cycle and pulse shape will be determined empirically. Equation (1) will be used for guidance in the welding parameter search.

NEUTRON ACTIVATION ANALYSIS

The initial postulated use for the blow-molded tLCP pressure vessels is for propellant storage. Typical propellants envisioned for use are hydroxylammonium nitrate/triethanolamine nitrate (HAN/TEAN) storable liquids, hydrogen peroxide, oxygen, kerosene, and, potentially, deuterium and nitrogen trifluoride or fluorine.

The first concern is to ascertain if anything is present within the plastic structure that would cause an unwanted chemical reaction. Of the mentioned propellants, only two (HAN/TEAN and hydrogen peroxide) present any potential catalytically reactive problems.

Neutron activation analysis was conducted at the McClellan Nuclear Radiation Center. A number of synthesized and thermally-processed tLCPs were analyzed by gamma spectroscopy. The specimens were exposed to a thermal neutron fluence of 1.7×10^{12} n/cm^2. Only one catalytically active element was observed for the VECTRA resins (most probable for future blow-molding work)—manganese. The bulk concentration of manganese was 0.58 parts per billion in VECTRA A950, and 0.055 parts per billion in VECTRA B950. These values are a factor of 1000 below the values that would create a concern in long-term storage for either of the two mentioned propellants.

The results of the gamma spectroscopy clearly show that these polymeric materials are ideal candidates for any propellant that is susceptible to catalytic decomposition by heavy metal contamination.

CHEMICAL COMPATIBILITY OF LIQUID CRYSTAL POLYMERS

Even with the results of the neutron activation analysis, actual chemical compatibility testing was conducted using a HAN/TEAN liquid gun propellant, XM-46. Injection-molded tensile bars were dried overnight at 150°C and weighed. These specimens were then immersed in the HAN/TEAN propellant at 18-24°C; they were removed at intervals, rinsed, dried for one hour at 150°C, equilibrated, then weighed. Table 1 shows the results of the first 26 days of testing.

TABLE 1. Results of HAN/TEAN Compatibility Testing—Gravimetric Values of Liquid Crystal Polymer Tensile Bars as a Function of Immersion Time.

Soak Duration, hr	A950 Neat, g	A130 30% Glass, g	B130 30% Glass, g	B230 30% Carbon Fiber, g
0	6.80274	8.22429	8.54931	7.21413
20.4	6.80268	8.22437	8.54930	7.21400
113.6	6.80270	8.22437	8.54924	7.21389
140.3	6.80280	8.22452	8.54979	7.21413
161.8	6.80257	8.22433	8.54976	7.21400
185.8	6.80253	8.22432	8.54988	7.21393
209.3	6.80237	8.22411	8.54955	7.21365
308.1	6.80274	8.22554	8.54995	7.21413
620.3	6.80253	8.22427	8.54951	7.21387
1204.5	6.80271	8.22444	8.55015	7.21422
1441.5	6.80259	8.22438	8.54989	7.21413
5832.0	6.80288	8.22471	8.55135	7.21481

The A950 resin sample was injection molded from a pure VECTRA A resin; the A130 sample was molded from a VECTRA A resin that was loaded with 30% chopped glass fiber; the B130 sample was molded from a VECTRA B resin loaded with 30% chopped glass fiber; and the B230 sample was molded from a VECTRA B resin loaded with 30% graphite fiber. All of these resins are articles of commerce and were, therefore, easily obtainable.

As can be seen, all of the samples show variance that is well within experimental error; no increasing or decreasing weights are evident. The typical variance is on the order of 0.005%. Moreover, the liquid gun propellant shows no sign of degradation after contact with the polymer samples. This compatibility test will be continued over the next year to assess long-term storage compatibility with VECTRA polymers.

BARRIER PROPERTIES OF BLOW-MOLDED PARTS

Blow-molded VECTRA components were studied by the Hoechst Celanese Corporation in 1991. The summarized test results are included in this report as Appendix C. The results indicate pressure vessels thermally formed from VECTRA can meet a target leak rate of 1.0×10^{-5} cm^3 (STP)/s cm^2 for oxygen, nitrogen, hydrogen, carbon dioxide, helium, and argon, with a minimum wall thickness of 0.050 inches. The cases studied were at 1000, 2000, and 4500 psig. The gas transport properties were also found to be a function of the low solubility of the gas in the polymer rather than low transport mobility.

It has been established that tLCPs have extremely low reactivity to chemical species (Reference 1) and have excellent cryogenic properties (Reference 3). Propellant, or lasing fluid storage, is, thus, predominantly a function of permeability. Table 2 shows values for the species of interest.

TABLE 2. Diffusion Values for Species of Interest.

Species	Diffusion Coefficient, 10^{10} cm^2/s	{Molecular Weight}$^{1/2}$
Helium	7680	2.00
Hydrogen	966	1.42
(Deuterium)	-0-	2.01
Nitrogen	5.23	5.29
Argon	1.08	6.32
Oxygen	0.82	5.66
(Fluorine)	-0-	6.16
Carbon Dioxide	0.71	6.63
(Nitrogen Trifluoride)	-0-	8.43

Gaseous diffusion theory states that diffusion varies inversely with the square root of the molecular weight. This seems to correlate well within the table with the notable exceptions of the noble gases, helium and argon. The species in parentheses are proposed storable lasing gases, included for comparison.

More work will need to be done to be able to compare tanks made with tLCPs to conventional composite tanks and metallic containers. The data contained in Appendix C is highly encouraging for long-term storage of propellants and lasing gases.

CONCLUSIONS

The tLCP class of polyesters looks excellent for energetic material storage. Low permeation rates, inertness, high specific strength, rapid processing, and amenability to laser post-processing all add up to high-performance, low-cost pressure vessels for aerospace applications.

Preliminary work has shown that the VECTRA class of polyesters can be blow-molded. This implies that thermally-driven convolute winding technology could be a reality within the next calendar year. The VECTRA class of liquid crystal polyesters has proven to be compatible with HAN/TEAN-based liquid gun propellants and is highly recommended for containment.

RECOMMENDATIONS

It is recommended that a development program targeted at developing a storable propellant container be initiated. It is also recommended that a blow-molding process be coupled with annealing to form a propellant pressure tank. An effort in parallel must be initiated to explore thermally-driven filament- and/or convolute-winding using laser radiation.

In order to effect the above, a parametric study of laser welding of VECTRA needs to be carried out. The continuous wave laser exposure dose for surface degradation has to be measured. This is a key measurement because it will reflect how efficient the detuning of the polymer absorption spectrum is upon melting. It will give a good indication of achievable weld depth and weld speed.

The effect of gravity on welding should be investigated. Will an inverted geometry lead to seam depletion? This is not the case for polypropylene, but it could be a problem for a liquid crystal polymer. In this case, the low melt viscosity could be unfavorable.

Joint strength needs to be tested. Strength test results should be used as a feedback for optimizing weld conditions, in particular weld depth and maximum surface temperature.

Friction welding should also be carried out. It will provide a baseline against which laser welding will be evaluated.

REFERENCES

1. Phillips Laboratory. *Proceedings of the First Annual Advanced Polymer Components Symposium,* by J. J. Rusek. Phillips Laboratory, Edwards Air Force Base, Calif. (PL-TR-92-3018, publication UNCLASSIFIED.)

2. Phillips Laboratory. *Proceedings of the Second Annual Advanced Polymer Components Symposium,* by J. J. Rusek. Phillips Laboratory, Edwards Air Force Base, Calif., July 1992. (PL-TR-92-3018, Part II, publication UNCLASSIFIED.)

3. Phillips Laboratory. Advanced Polymer Components: Final Report, by J. J. Rusek. Phillips Laboratory, Edwards Air Force Base, Calif., October 1995. (PL-TR-95-3034, publication UNCLASSIFIED.)

4. Air Force Institute of Technology. *Design of an Air-To-Air Missile Incorporating LCPs, Master's Theses,* K. F. Byard et al. (AFIT/GSE/ENY/91D-1, publication UNCLASSIFIED.)

5. C. L. Frank. "Advanced Polymer Processing and Mold Design," in *Proceedings of the First Annual Advanced Polymer Components Symposium,* PL-TR-92-3018, Part II, pp. 451-456. Paper UNCLASSIFIED.

6. C. Ruffler and K. Giirs, *Optics Laser Technol.* **4**, 265 (1972); W. W. Duley and J. N. Gonslaves, *Can. Res. and Development,* January 1972, pp. 25-29.

7. W. W. Duley and R. E. Mueller, *Polym. Eng. and Science* **32**, 582 (1992).

8. P. A. Atanasov, *Opt. Eng.* **34**, 2976 (1995).

9. B. G. Sumpter, G. A. Voth, D. W. Noid, and B. Wunderlich, *J. Chem. Phys.* **93**, 6081 (1990).

10. C. J. Nonhof, *Polym. Eng. and Science* **34**, 1547 (1994).

Appendix A
ADVANCED POLYMER COMPONENTS PUBLICATIONS; SUMMARY OF CONTENTS

PROCEEDINGS OF THE FIRST ANNUAL ADVANCED POLYMER COMPONENTS SYMPOSIUM [PL-TR-92-3018]

SUMMARY OF CONTENTS

PART DESIGN, C. Frank, ACPO, McClellan AFB
PROCESS RESEARCH, N. Schott, University of Massachusetts at Lowell

LOW TEMP CVD/COMPATABILITY, E. Wucherer, Phillips Laboratory, Edwards AFB

2X4 MOTOR, H. Nguyen, Phillips Laboratory, Edwards AFB

LASER EARTH TO ORBIT VESSEL, J. Kare, Lawrence Livermore National Laboratory

FLIGHT LOGISTICS APPLICATIONS, S. Hardy, Hill AFB

RETROFIT APPLICATIONS, T. Fuchser, Arnold Engineering Development Center

RETICULATED BONDLINE, K. Mahaffy, Phillips Laboratory, Edwards AFB

PROCEEDINGS OF THE SECOND ANNUAL ADVANCED POLYMER COMPONENTS SYMPOSIUM [PL-TR-92-3018, PART II; V1,V2,V3]

SUMMARY OF CONTENTS

Development and Testing of a Curved Mica X-Ray Focusing Spectrometer for Extended X- Ray Absorption Fine Structure Studies
C. Zorman; G. DeRose; R. Hoffman, Case Western Reserve University

Characterization, FDEMS Sensing and In Situ Process Monitoring of the Physical Changes Occurring with Time and Temperature During Cure of High Temperature Liquid Crystal Thermotropes
D. Kranbuehl; B. Kipp, College of William and Mary

Structure- Property Relationships of *VECTRA* Liquid Crystal Polymers
L. Sawyer, Hoechst-Celanese Corporation

Volume 3

Contrasting Shear- Flow Behavior of Tumbling and Flow-Aligning Nematics
P Mather; D. Pearson; R. Larson, University of California at Santa Barbara

Wiley Organics and Organic Technologies
J. Etheridge, Organic Technologies

Hybrid Sounding Rocket Development at the Unite States Air Force Academy
M. Lydon; R. Simmon, United States Air Force Academy

Investigation of the Annealing Effects on *DUPONT HX-4000* Liquid Crystalline Polymer
M. Lindauer; S. Small, Loyola Marymount University

Advanced Polymer Processing and Mold Design
C. Frank, ACPO, McClellan AFB

Final Report of *Predator* Motorcase Adhesive Bonding Screen
B. Guest, Naval Air Warfare Center, China Lake

Modern Ablatives. The Design, Development, and Application of Hybrid Polymers
J. Lichtenhan, Phillips Laboratory, Edwards AFB

A Preliminary Investigation Into the Nature of a Graded Propellant/insulation Interface in Solid Rocket Motors
C. Noel, Ohio State University; J. Lichtenhan, Phillips Laboratory, Edwards AFB

Design and Analysis of the Air Force Academy Solid Booster
T Elkins, Phillips Laboratory, Edwards AFB

Liquid Crystal Polymer AFA Booster Motor Development: Propellant Development, Motor Design and Preliminary Testing
H. Nguyen, Phillips Laboratory, Edwards AFB
APD: Hoechst Celanese LCP Property Data

ADVANCED POLYMER COMPONENTS : FINAL REPORT [PL-TR-95-3034; V1,V2]

SUMMARY OF CONTENTS

Liquid Crystal Polymer's Suitability for MMH and NTO Turbopump Applications
T. R. Hill, Phillips Laboratory, Edwards AFB

Volume 2
Cryogenic Testing of Liquid Crystal Polymers
J. Phillips, Phillips Laboratory, Edwards AFB

USAF Turbopump Plastics Testing: Oxygen Exposure
H. D. Beeson, R. Shelley, NASA White Sands Test Facility

Tensile Testing of Liquid Crystal Polymers in Liquid Hydrogen
T. J. Eisenreich, General Dynamics Space Systems Division

Tensile Testing of Liquid Crystal Polymers
T. Reed, Phillips Laboratory, Edwards AFB

Injection Molded Rocket Motor Case
C. L. Frank, USAF ACPO, McClellan AFB

Hybrid Nozzle Demonstrator
E. Schmidt, Phillips Laboratory, Edwards AFB

Test Data from the Firings of Two Stainless Steel and Two Liquid Crystal Polymer Case Motors
A. Kenney, Phillips Laboratory, Edwards AFB

Further Testing of *VECTRA* 2 x 4 Motor Cases
H. T. Nguyen, Phillips Laboratory, Edwards AFB

Development and Testing of Liquid Crystal Polymer Solid Rocket Motors
T. R. Reed, Phillips Laboratory, Edwards AFB

Development and Testing of Liquid Crystal Polymer Solid Rocket Motors and Hydrostatic Testing of Liquid Crystal Polymer Rocket Motor Cases
T. R. Reed, Phillips Laboratory, Edwards AFB

Charred Plastic Tube Specimen Microstructural Evaluation
J. Meininger, McClellan AFB

Solid Rocket Propulsion Applications for Advanced Polymers
J. Chew, J. Rusek, Phillips Laboratory, Edwards AFB

Propulsion Applications for Thermotropic Liquid Crystal Polymers
J. Shelley, Phillips Laboratory, Edwards AFB

Design of a Blow Molded LCP Pressure Vessel and a Fiber Reinforced Pressure Vessel
G. J. Price, Phillips Laboratory, Edwards AFB

Appendix B
LASER HEATING OF SOLIDS

LASER HEATING OF SOLIDS

AN INTRODUCTION TO THE ELEMENTARY THEORY THAT PERTAINS TO THE HEATING OF SOLIDS WITH LASERS. IT IS BASED ON SOLVING THE HEAT DIFFUSION EQUATION. EMPHASIS IS ON SIMPLE ANALYTICAL MODEL THAT CAN PROOVE VERY VALUABLE TO THE EXPERIMENTALIST IN TRYING TO SET UP A SYSTEM FOR LASER WELDING OR LASER MACHINING OF A GIVEN MATERIAL. FOR A MORE DETAILED TREATMENT, THE READER SHOULD CONSIDER CURRENT COMPUTER SIMULATIONS.

Printed September 15, 1996.

P.O. BOX 2683 LANCASTER CA 93539-2683 (805) 940-0466

CONTENT

LASER HEATING OF SOLIDS

I. HEAT FLOW PROBLEM (CARSLAW AND JAEGER [1])

The equation for heat flow in a 1D solid is

$$\rho C(\partial T/\partial t) = (\partial/\partial z(K\partial T/\partial z)) + \Phi(z,t) \qquad (1)$$

where

ρ = material density, gm/cm^3

K = thermal conductivity, W/cm°C

C = heat capacity, J/gm°C

are material properties which depend upon temperature and position. $\Phi(z,t)$ is the rate at which heat is supplied to the solid per unit time per unit volume in J/sec cm^3 and T(z,t) is the resulting temperature distribution in the solid.

Difficulties:
- -T dependence of thermal properties.
- -T dependence of optical properties.
- -Phase changes.

Simplifications:
- -Usually thermal properties do not depend steeply on T, i.e. use average values.
- -Solve each phase separately, including latent heat required when needed.
- -Assume homogeneous, isotropic material.

The resulting equation is

$$\nabla^2 T - 1/\kappa(\partial T/\partial t) = -\Phi(x,t)/K \qquad (2)$$

where

$\kappa = K/\rho C$ = thermal diffusivity, cm^2/sec.

II. THERMAL DIFFUSIVITY

A simple dimensional analysis shows that

$(\kappa t)^{1/2}$ = thermal diffusion depth, cm.

It is often useful to compare it with optical absorption depth. For a laser pulse of length t_p

$$z_{1/e} = 2(\kappa t_p)^{1/2} \qquad (3)$$

is the distance from the surface at which T is 1/e of the value at z = 0. This correponds to a heat release of $2\rho C T_0(\pi\kappa)^{1/2}$ per unit area at the plane z = 0 at t = 0. The heat per unit area absorbed is $It_p\alpha$ where I = laser intensity, W/cm^2 and α = absorptance of the material. Thus we have

$$It_p\alpha = 2\rho C T_0(\pi\kappa)^{1/2} \text{ or } T_0 = (It_p\alpha)/(2\rho C(\pi\kappa)^{1/2})$$

and

$$T(z,t) = ((It_p\alpha)/(\rho C\pi^{1/2}))\exp(-(z^2)/(4\kappa t))/(4\kappa t)^{1/2} \qquad (4a)$$

for t larger than 0.

Equation (4a) can be rewritten

$$T(z,t) = ((It_p\alpha)/(\rho C\pi^{1/2}))\exp(-z^2/z_D^2)/z_D \qquad (4b)$$

where $z_D = 2(\kappa t)^{1/2}$ is a thermal diffusion depth.

III. IRRADIATION WITH A UNIFORM BEAM OF A SEMI INFINITE SLAB

Case of uniform beam.

Incident power given by

$P_0(t) = 0$ for t less than 0
$P_0(t) = P_0$ for t equal or greater than 0

The beam radius is ω, cm. For sufficiently short exposure, or small thermal diffusivity, z_D is much smaller than ω. In this case

$$T(0,t) = (\alpha P_0 z_D)/(\pi\omega^2 K) \qquad (5)$$

and

$$T(0,inf) = (\alpha P_0)/(\pi\omega K) \qquad (6)$$

P_0/ω defines the maximum achievable temperature. Duley [2] gives the minimum value needed to melt the surface of a solid metal with a CO_2 laser, using a circular beam.

Material	P_0/ω (10^4 W/cm)
Al	13
Cu	34
Sn	0.85
Ni	4.4

Numerical examples.

Comparison between a conducting metal like Al, a not very conducting metal like 304 SS, and a non conducting material like carbon phenolic. Use a CO_2 laser for heating with a 0.2 cm beam radius and 50 W of CW power, i.e. a non focused table top system.

Material	α	K (W/cm°C)	κ (cm^2/sec)
Aluminum	0.1	2	0.74
304 SS	0.1	0.26	0.054
Carbon Phenolic	1	0.01	0.004

Using equation (6) we have

	Al	304 SS	Carbon Phenolic
T(0,inf) (°C)	23.5	47.1	7074

Aluminum barely notices the influence of the laser, 304 SS warms up slightly, but carbon phenolic vaporizes! Note that the laser power, and the beam radius factor in linearly.

Time for melting or for vaporizing.

Recalling equation (5), and using $T_m = T(0,t)$, we have

$$t_m = (\pi^3\omega^4K^2T_m^2)/(4\alpha^2P_0^2\kappa) \qquad (7a)$$

and

$$t_v = (\pi^3\omega^4K^2T_v^2)/(4\alpha^2P_0^2\kappa) \qquad (7b)$$

The power dependence on the beam radius explains the importance of focusing on the effect of the laser on the material of interest. Equations (7a,b) are very useful from a practical stand point since they allow the experimentalist to adjust the optics to produce the desired effect with a given laser system.

Heating and cooling rates.

A: Optical absorption depth much smaller than heat diffusion length (i.e. most metals from the UV to the IR for short pulses.)

$\Delta T = (\alpha I_0 t_p)/(\rho C(\kappa t_p)^{1/2})$ is the temperature rise due the the absorption of a fraction of the laser energy during the pulse by a layer of material of which thickness depends on heat diffusion.

The heating/cooling rate is

$$\Delta T/t_p = (\alpha I_0)/(\rho C(\kappa t_p)^{1/2}) \qquad (8)$$

B: The optical penetration length is larger than the diffusion length (i.e. most organic polymers in the IR.)

Use Beer's law

$$I = I_0 \exp(-\alpha z) \qquad (9)$$

The heat absorbed is (1-R)I where R is the reflectivity, over a depth α^{-1}. Thus the temperature distribution is approximately

$$\Delta T = (\alpha(1-R)I_0 t_p)\exp(-\alpha z)/(\rho C) \qquad (10)$$

and the heating rate is

$$\Delta T/t_p = (\alpha(1-R)I_0)\exp(-\alpha z)/(\rho C) \qquad (11)$$

To evaluate the cooling rate, we assume that after the pulse, the heat diffuses about α^{-1}. Thus, the cooling time t_c is about $(\alpha^{-1})^2/\kappa$. The cooling rate at the surface is

$$\Delta T/t_c = (\alpha^3(1-R)I_0 \kappa t_p)/(\rho C) \qquad (12)$$

Case of annealing.

The surface temperature should not exceed the melting point, i.e. the melting is reached at the end of the pulse when $t = t_p$.

$$dT/dt = T_m/t_p \qquad (13)$$

If one heats Al up to its melting point with a 10 nsec pulse from a Q switched Nd:YAG laser, the heating rate is 6.4×10^{10} °C/sec.

IV. LASER DRILLING (HARRACH [3])

The laser impinges on the material surface (z = 0) at time t = 0. A fraction α of the energy is absorbed. The surface temperature rises, and a temperature distribution T(z,t) arises in the solid due to thermal conduction.

For machining purpose, the intensity of the laser should be high enough to melt the surface and to vaporize it. A crater forms at the surface and some material is ablated, as the vapor-solid boundary moves back into the material.

This problem can be divided into 3 phases according to phase transformation on the front and back of the material slab.

$t = 0$	Irradiation begins
$t = t_l$	The back surface warms up considerably
$t = t_v$	The front surface starts to vaporize
$t = t_{BT}$	The back surface begins to melt or burn through occurs

Assumptions.

-Thermal and optical parameters are constant.
-T variations in a single condensed phase to be found.
-Longitudinal heat conduction is only loss mechanism.
-Absorption occurs in a very thin layer.
-Vapor blow-off plume cool enough to be transparent to the laser.

Prevaporization phase.

t is less than t_l.

$$T(z,t) = T(0,t)(1-z/\delta(t))^2\exp(-z/\delta(t)) \quad (14)$$

for z less than $\delta(t)$

$$T(z,t) = 0 \text{ for } z \text{ more than } \delta(t)$$

where $\delta(t)$ is a thermal penetration depth.

For step function irradiation (CW mode)

$$T(0,t) = 1.12(\alpha_0 I_0/K)(\kappa t)^{1/2} \quad (15)$$

$$\delta(t) = 3.37(\kappa t)^{1/2} \quad (16)$$

Find t_1 and t_v.

$\delta(t_1) = 1 = 3.37(\kappa t_1)^{1/2}$, thus

$$t_1 = 0.0881^2/\kappa \qquad (17)$$

when t_1 is less than t_v, i.e. the front surface does not vaporize before the back surface heats up.

Similarly, $T_v = 1.12(\alpha_0 I_0/K)(\kappa t_v)^{1/2}$, thus

$$t_v = 0.79T_v^2K^2/(\kappa I_0^2) \qquad (18)$$

when t_v is less than t_1, i.e. back surface heating does not need to be taken into account.

Case when t_1 is less than t_v.

$$T(0,t) = 0.245(\alpha_0 I_0/K)(0.736\kappa t/1^2 + 1) \qquad (19)$$

and

$$T(1,t) = 0.088(\alpha_0 I_0 1/K)(11.35\kappa t/1^2 - 1) \qquad (20)$$

thus, setting $T(0,t) = T_v$ defines the vaporization time as

$$t_v = (KT_v1)/(\kappa\alpha_0 I_0) - 0.2451^2/\kappa \qquad (21)$$

Let $T'_m = T_m(1+(L_m/(CT_m)))$, where L_m is the latent heat of melting and T_m is the actual melting temperature. T'_m is an effective melting temperature. The burn through temperature is defined by setting $T(1,t) = T'_m$. The burn through time is

$$t_{BT} = 0.0881^2/\kappa + (1KT'_m)/(\kappa\alpha_0 I_0) \qquad (22)$$

which holds when the surface does not vaporize before melt through occurs.

Post vaporization phase.

Case of a semi infinite slab. Vaporization of the surface occurs before melt through.

$z_s(t)$ = the position of the front surface
$d(t)$ = thermal penetration length from z_s

The temperature distribution in the material is

$$T(z,t) = T_v(1-(z-z_s(t))/d(t))^2\exp(-(z-z_s(t))/d(t)) \qquad (23)$$

when $z-z_s$ is less than $d(t)$, and $T(z,t) = 0$ when $z-z_s$ exceeds $d(t)$, i.e. the heat has not reached that region yet.

Speed of vaporization.

Recall equation (7b)

$$t_v = (\pi^3\omega^4K^2T_v^2)/(4\alpha^2P_0^2\kappa) \qquad (7b)$$

The volume vaporized per unit time is

$$V = \pi\omega^2\dot{z}_s(t) \qquad (24)$$

requiring

$$Q = \pi\omega^2\dot{z}_s(t)(\rho CT_v + L) \qquad (25)$$

amount of energy to be absorbed per unit time. Here L is the total latent energy.

The energy absorbed per second in the irradiated area is $\alpha I_0\pi\omega^2$, thus by setting $\alpha I_0\pi\omega^2 = \pi\omega^2\dot{z}_s(t)(\rho CT_v + L)$ we obtain

$$\dot{z}_s(t) = \alpha I_0/(\rho CT_v + L) \qquad (26)$$

This result is limited by how fast can the vaporized material leaves the vaporization surface.

Drilling depth.

Case of a CW laser.

$$l_{CW} = \dot{z}_s(t)t_{dw} = \alpha I_0^{CW}t_{dw}/(\rho CT_v + L) \qquad (27)$$

Case of a pulsed laser.
Need to sum up the depth provided by each pulse. Assume that for each pulse of length t_p, T_v is reached. The repetition rate is f. We have

$$l_p = \alpha I_0^P f t_p t_{dw}/(\rho CT_v + L) \qquad (28)$$

In general intensities achieved in pulsed mode are much larger than those of CW mode, however pulsed mode suffer from a

low duty cycle. Thus the choice of CW or pulsed mode to drill a material depends on the specifics of the problem, i.e. properties of the material and available laser system.

V. HEAT TREATING WITH A SCANNING LASER BEAM (CLINE AND ANTHONY [4])

Coordinate frame fixed on the material.

Laser impinges parallel to z axis on plane z = 0 at time t = 0. The laser moves in the +x direction with speed v.

Use a Gaussian beam intensity distribution, with total power P and radius ω.

$$\Phi = (h(z)\alpha P/2\pi\omega^2)\exp(-((x-vt)^2 + y^2)/(2\omega^2)) \qquad (29)$$

where h(z) = 1 for z in the range $0\text{-}\alpha^{-1}$, and h(z) = 0 for z outside that range.

The heat diffusion equation (2) is solved by superposition of the known solution for the thermal distribution of a unit point source on the surface (moving Green's function.)

Case of a moving point source.

$\omega = 0$ and

$$T = (P/(K2\pi r))\exp(-v(r + x)/2\rho\kappa) \qquad (30)$$

where $r = x^2 + y^2 + z^2$, i.e distance from the source. T is infinite at r = 0, and falls off with distance from the source.

Case of finite beam radius.

$$T(x,y,z) = (P/K\omega)\psi(x,y,z,v) \qquad (31)$$

where ψ is a distribution function.

Cline and Anthony [4] have plotted ψ versus x/ω^2 for different v and at different z for a single v. They also have plotted ψ versus $\omega v/(\rho\kappa)$ for different z, as well as ψ versus z/ω^2 for different v.

As v increases, the maximum temperature decreases and shifts behind the center of the moving laser. At increasing depths below the surface, the temperature decreases. The temperature under the laser beam decreases with increasing v, because less time is available to heat the material. The decrease in T for increasing z follows approximately an exponential decay.

Cooling rate.

$$\partial T/\partial t = -v(x/r^2 + (v/(2\rho\kappa))(1 + x/r))T \quad (32)$$

VI. MELTING WITH A SCANNING LASER

T_{max} is in the T_m-T_v range, but does not reach T_v.

The scanning laser produces a weld puddle that moves with the beam to melt and subsequently resolidify material near the surface.

The latent heat is absorbed and then liberated-minor effect on penetration depth. Not included in calculation.

Change of K not included.

Solid-liquid isotherm is

$$T_m = (P_m/K\omega)\psi(x,y,z,v) \quad (31b)$$

and

$$z_m = z_0 \ln(P/P_m) \quad (32)$$

defines the melting depth, where z_0 = penetration depth, and P_m = power required to reach melting.

VII. DEEP-PENETRATION WELDING (KLEMENS [5])

High laser power densities. Liquid T near T_v. Liquid zone extends deep into the material with respect to the weld width.

The vapor pressure pushes the liquid-vapor interface below the surface to z_v to form a keyhole for the laser beam to penetrate deeply into the material. The laser power is completely absorbed by the multiple reflections that occur in the cavity in the liquid.

Spherical heat flow in vapor protrusion ($z = z_v$). The pressure in the cavity is

$$p = \rho_l z_v g + (\gamma_{lv}/r_v) \quad (33)$$

where

ρ_l = density of the liquid

g = acceleration of gravity

γ_{lv} = surface tension at the liquid-vapor interface

r_v = radius of the vapor protrusion tip

Assume T of tip is T_v. Onset of deep-penetration occurs when the surface reaches T_v at P_v. Using $P/P_v = T/T_v$

$$P/P_v = (2z_v/z_0)(1-\exp(-2(z_v/z_0))) \qquad (34)$$

The keyhole depth increases from 0 as the laser power exceeds the vaporization minimum.

At high power level, the melt depth is at a fixed distance below the keyhole depth

$$z_m = z_v + z_0 \ln(T_v/T_m) \qquad (35)$$

When applied to 304 SS, calculated depths correlate well with experimental results up to depths of about 1 cm.

VIII. LIST OF SYMBOLS

ρ - material density
ρ_l- density in the liquid phase
K - thermal conductivity
C - heat capacity
T - material temperature
T_0- surface temperature
T_m- melting temperature
T_v- vaporization temperature
x - axis of laser motion
y - axis of material plane, orthogonal to x
z - laser beam axis, depth in the material
z_0- penetration depth
z_D- thermal diffusion length
z_m- melting depth
z_s- position of the vaporization surface
$\dot{z}_s$- rate of vaporization
z_v- vaporization depth
Φ - Rate of power absorbed per unit volume
κ - thermal diffusivity
t - time
t_p- length of laser pulse
t_c- Cooling time
t_l- time to heat back side of slab
t_m-time to melt the surface
t_v-time to vaporize the surface
t_{BT}-time to burn through the slab
I - laser intensity in the material
I_0- laser intensity at the surface
I_0^{CW}-CW laser intensity at the surface

I_0^p-pulsed laser intensity at the surface
α - fraction of laser energy absorbed or absorptance
R - fraction of laser energy reflected
α^{-1}-radiation penetration depth into the material
P - laser power
P_0- laser power at the surface
P_m- laser power to reach melting
P_v- laser power to reach vaporization
ω - beam radius
δ - thermal penetration depth
L_m- latent heat of melting
L_v- latent heat of vaporization
L - total latent heat
d - thermal penetration distance from z_s
l_{CW}-CW drilling depth
l_p- pulsed drilling depth
f - pulse repetition rate
Q - energy absorbed by the material
V - volume
v - laser beam speed along the x axis
r - distance from the impinging laser beam
r_v- vapor protrusion radius
ψ - temperature distribution function
γ_{lv}-surface tension at the liquid-vapor interface
g - acceleration of gravity

REFERENCES

-1. H.S. Carslaw and J.C. Jaeger, "COnduction of Heat in Solids", 2nd ed. (Oxford University Press (Clarendon), London and New York, 1959).

-2. W.W. Duley "CO_2 Lasers: Effects and Applications" (Academic Press, New York, 1976).

-3. R.J. Harrach, J. Appl. Phys. **48**, 2370 (1977).

-4. H.E. Cline and T.R. Anthony, J. Appl. Phys. **48**, 3895 (1977).

-5. P.G. Klemens, J. Appl. Phys. **47**, 2165 (1976).

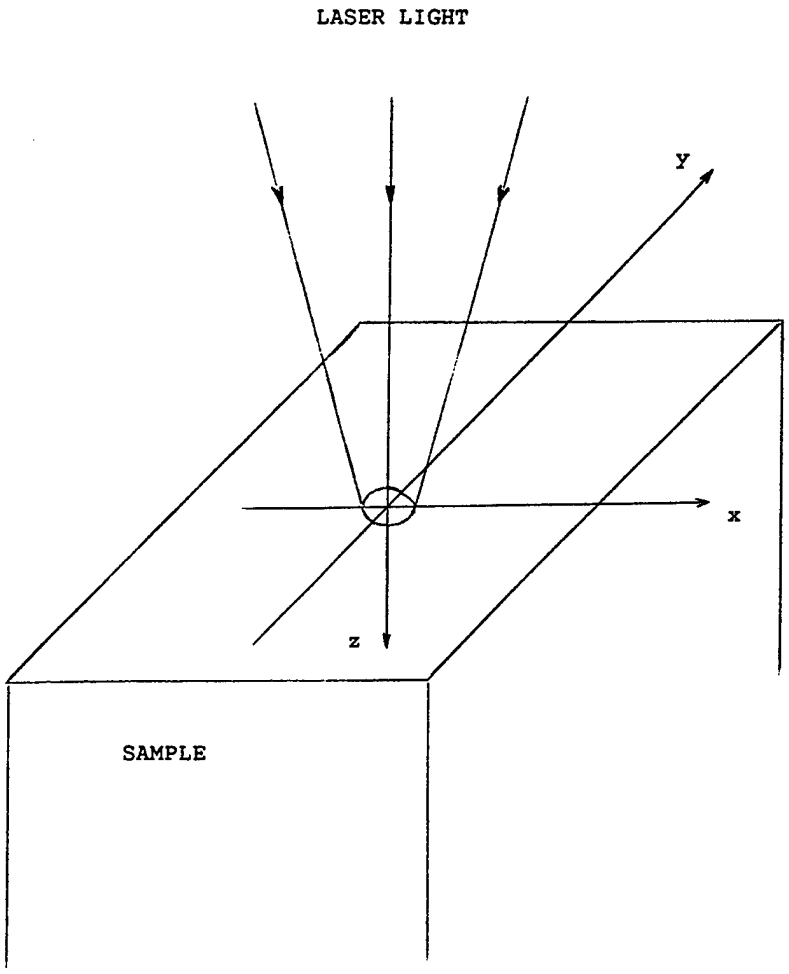

FIGURE 1. Irradiation geometry and coordinate axes.

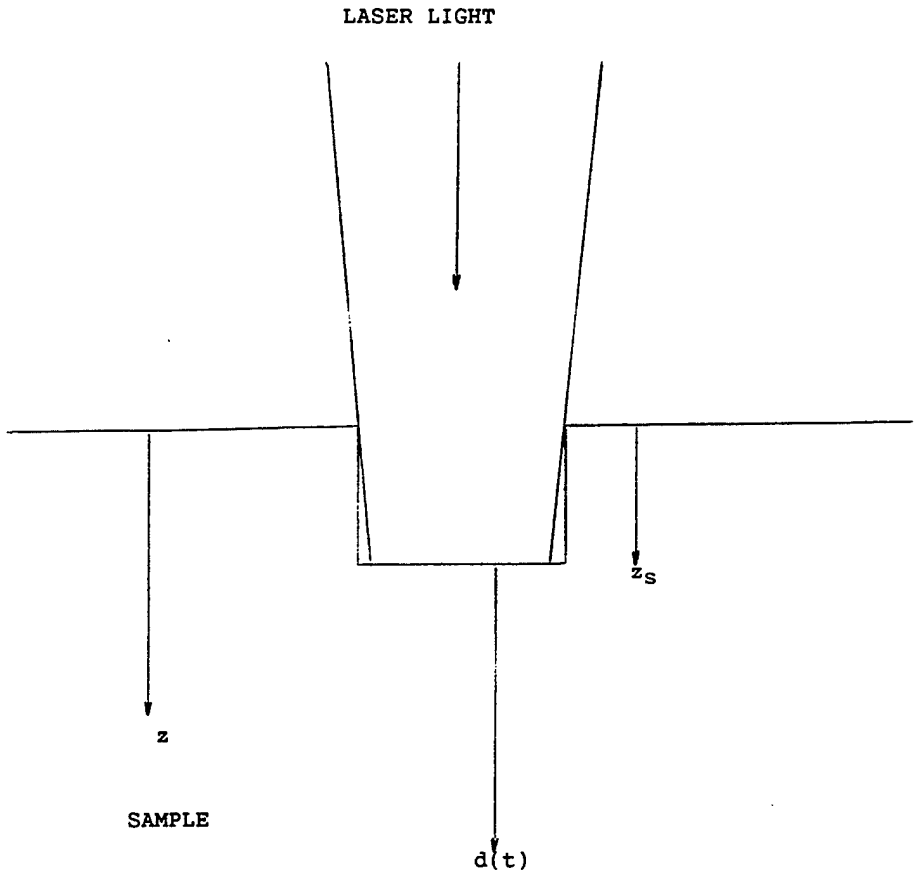

FIGURE 2. Definitions for the heat flow problem in the post vaporization problem.

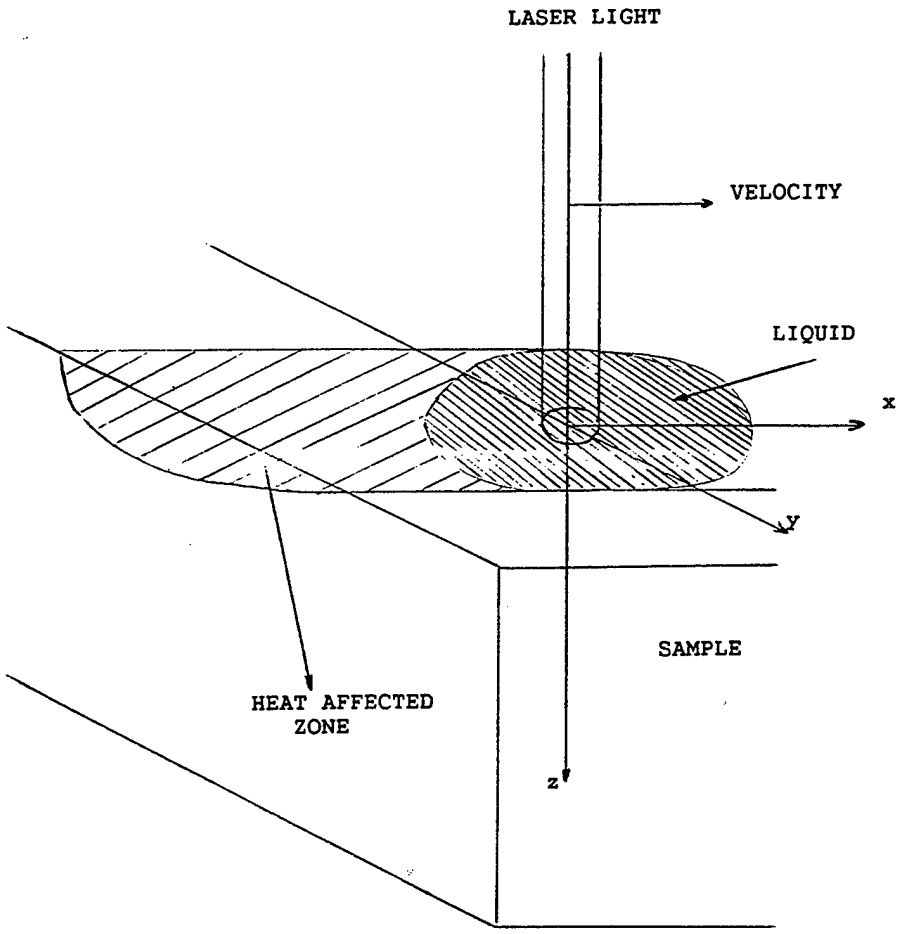

FIGURE 3. Schematic illustrating laser-beam heating by a scanning laser beam moving with constant velocity in the x direction.

Appendix C
EFFECTIVENESS OF VECTRA AS A HIGH PRESSURE BARRIER MATERIAL

Interoffice Memo

Hoechst Celanese

Date: August 1, 1991 FJO-91-06

To: Steve Blake From: Frank Onorato

Dept/Location: Charlotte Dept/Location: Summit

Subject: The Effectiveness of Vectra as a High Pressure Barrier Material

cc: P. Foley
L. Sawyer
R. Straff
J. Shepherd

I have completed the calculations to determine the permeability behavior of Vectra for use in high pressure gas container applications. The results indicate that a Vectra pressure vessel can meet the revised target leak rate of 1.0×10^{-5} cc(STP)/sec for all of the specified gases (hydrogen, helium, oxygen, nitrogen, argon, and carbon dioxide) with a minimum wall thickness of 50 mils. However, the original leak rate specification of 1.0×10^{-9} cc(STP)/sec can only be met by oxygen, nitrogen, argon, and carbon dioxide when the vessel wall thickness is at least 100 mils. The leak rate for helium (143×10^{-9} cc(STP)/sec cm^2) and hydrogen (39×10^{-9} cc(STP)/sec cm^2) fail to meet the leak rate originally specified even when the largest wall thickness was assumed (250 mils).

The calculations were based on four values for the wall thickness (20, 50, 100, and 250 mils), three pressures (1000 psig, 2500 psig, and 4500 psig), and six gases (helium, hydrogen, oxygen, nitrogen, argon, and carbon dioxide). The nonsteady state solution to the diffusion equation was used to calculate the leak rate cc(STP)/sec cm^2 as a function of time, and total volume of gas permeated cc(STP)/cm^2 as a function of time for each combination of wall thickness, pressure, and gas. Although the initial concentration of penetrant within the film was assumed to be zero (cc(STP)/cc polymer) the solution to the Fickian nonsteady state diffusion equation does allow this initial concentration to be specified. If required, the calculations can be repeated with a nonzero value. A summary of the results are presented in Tables I-IV. I have also included the detailed results obtained for each individual case. They are contained in the 144 plots which have been attached.

Table I contains the values of the diffusivity and solubility coefficients used in the calculations along with the permeability coefficients. Table II summarizes the time required for the vessel to reach a steady state leak rate, and Table III summarizes the values of the steady state leak rates. The leak rate is presented as a factor of 10^{-9} since this was the initial target for the leak rate.

The time to steady state is a function of the diffusion coefficient and the film thickness. For very thick films, or very low diffusion coefficients the leak rate versus time curve will initially be

Hoechst

nonlinear. During this time period the average value for the leak rate will be less than the steady state value. For example, a 100 mil thick sample of Vectra when pressurized with nitrogen will take approximately fifteen years to reach its steady state leak rate, while a 100 mil thick sample of Vectra when pressurized with helium, will take approximately twelve hours to reach its steady state leak rate. If the lifetime of a container is five years then even though the steady state leak rate for nitrogen may exceed specifications, the effective leak rate (total gas permeated in five years) may meet specifications. For this reason I have included plots of the total volume of gas permeated per square centimeter as a function of time. These results are summarized in Table IV.

The values displayed in Table IV were arrived at by assuming the lifetime of a container would be five years. The effective leak rate over that time period was then calculated by using the volume of gas permeated/cm^2 versus time plots. By comparing the results summarized in Tables II and IV it is clear that the difference between the effective leak rate and the steady state leak rate can be considered. The exception being hydrogen and helium were the time to steady state is very short.

Frank Onorato

Enclosure
FJO:djd

TABLE I
VALUES OF DIFFUSIVITY AND SOLUBILITY USED IN THE CALCULATIONS

GAS	PERMEABILITY COEFFICIENT * 10^5 x barrer	DIFFUSION COEFFICIENT 10^{10} cm^2/sec	SOLUBILITY COEFFICIENT ** 10^4 x $cm^3(stp)/cm^3$ cm Hg
HELIUM	17357.0	7680.0	0.226
HYDROGEN	4636.0	966.0	0.48
NITROGEN	3.55	5.23	0.883
OXYGEN	46.18	0.82	0.433
ARGON	9.85	1.08	0.912
CARBON DIOXIDE	73.84	0.71	10.4

* 1 barrer = 10^{-10} cc(stp)cm/cm^2 sec cm Hg, $P = D^*S$

** SOLUBILITY COEFFICIENT ORIGINALLY REPORTED BY DR. PAUL IN UNITS OF CC(STP)/CC ATM

TABLE II
TIME TO ESTABLISH A STEADY STATE LEAK RATE AS A FUNCTION OF WALL THICKNESS

FILM THICKNESS MILS	HELIUM TIME TO STEADY STATE	HYDROGEN TIME TO STEADY STATE	OXYGEN TIME TO STEADY STATE	NITROGEN TIME TO STEADY STATE	ARGON TIME TO STEADY STATE	CARBON DIOXIDE TIME TO STEADY STATE
250	4.0 DAYS	30 DAYS	15 YEARS	100 YEARS	70 YEARS	100 YERAS
100	0.5 DAYS	5 DAYS	2 YEARS	15 YEARS	10 YEARS	15 YEARS
50	4 HOURS	1 DAY	7 MONTHS	4 YEARS	3 YEARS	4 YEARS
20	40 MINUTES	4 HOURS	30 DAYS	8 MONTHS	6 MONTHS	8 MONTHS

THE STEADY STATE LEAK RATE AS A FUNCTION OF WALL THICKNESS AND GAS PRESSURE

TABLE IIIA $\Delta P = 1000$ psig

FILM THICKNESS MILS	HELIUM LEAK RATE x 10^9 cc/sec cm^2	HY DROGEN LEAK RATE x 10^9 cc/sec cm^2	OXY GEN LEAK RATE x 10^9 cc/sec cm^2	NITROGEN LEAK RATE x 10^9 cc/sec cm^2	ARGON LEAK RATE x 10^9 cc/sec cm^2	CARBON DIOXIDE LEAK RATE x 10^9 cc/sec cm^2
250	143	38.63	0.3816	0.02934	0.08139	0.6102
100	359	96.59	0.9541	0.07335	0.2035	1.525
50	717	193.2	1.908	0.1467	0.4070	3.051
20	1793	482.9	4.770	0.3667	1.0174	7.627

TABLE IIIB $\Delta P = 2500$ psig

FILM THICKNESS MILS	HELIUM LEAK RATE x 10^9 cc/sec cm^2	HY DROGEN LEAK RATE x 10^9 cc/sec cm^2	OXY GEN LEAK RATE x 10^9 cc/sec cm^2	NITROGEN LEAK RATE x 10^9 cc/sec cm^2	ARGON LEAK RATE x 10^9 cc/sec cm^2	CARBON DIOXIDE LEAK RATE x 10^9 cc/sec cm^2
250	336	95.8	0.9458	0.0727	0.2017	1.512
100	889	239	2.364	0.1818	0.5043	3.781
50	1777	479	4.729	0.3636	0.1009	7.561
20	4443	1197	11.822	0.9089	2.5210	18.90

TABLE IIIC $\Delta P = 4500$ psig

FILM THICKNESS MILS	HELIUM LEAK RATE x 10^9 cc/sec cm^2	HY DROGEN LEAK RATE x 10^9 cc/sec cm^2	OXY GEN LEAK RATE x 10^9 cc/sec cm^2	NITROGEN LEAK RATE x 10^9 cc/sec cm^2	ARGON LEAK RATE x 10^9 cc/sec cm^2	CARBON DIOXIDE LEAK RATE x 10^9 cc/sec cm^2
250	638	172	1.698	0.1305	0.3621	2.715
100	1595	430	4.245	0.3264	0.9054	6.787
50	3191	860	8.490	0.6527	1.811	13.58
20	7977	2149	21.22	1.6320	4.527	33.94

THE ESTIMATED AVERAGED LEAK RATE AFTER 5 YEARS OF OPERATION

TABLE IVA $\Delta P = 1000$ psig

FILM THICKNESS MILS	HELIUM LEAK RATE x 10^9 cc/sec cm^2	HY DROGEN LEAK RATE x 10^9 cc/sec cm^2	OXY GEN LEAK RATE x 10^9 cc/sec cm^2	NITROGEN LEAK RATE x 10^9 cc/sec cm^2	ARGON LEAK RATE x 10^9 cc/sec cm^2	CARBON DIOXIDE LEAK RATE x 10^9 cc/sec cm^2
250	143	38.63	0.095	0.0063 *	0.0063	0.028 20 **
100	359	96.59	0.856	0.0139	0.063	0.317
50	717	193.2	1.408	0.0951	0.285	2.22
20	1793	482.9	4.770	0.317	0.92	6.97

TABLE IVB $\Delta P = 2500$ psig

FILM THICKNESS MILS	HELIUM LEAK RATE x 10^9 cc/sec cm^2	HY DROGEN LEAK RATE x 10^9 cc/sec cm^2	OXY GEN LEAK RATE x 10^9 cc/sec cm^2	NITROGEN* LEAK RATE x 10^9 cc/sec cm^2	ARGON LEAK RATE x 10^9 cc/sec cm^2	CARBON DIOXIDE LEAK RATE x 10^9 cc/sec cm^2
250	356	95.8	0.28	0.00317 *	0.0211	0.032
100	889	239	2.03	0.0044	0.190	0.95
50	1777	479	4.729	0.0266	0.793	5.07
20	4443	1197	11.822	0.847	2.28	15.8

TABLE IVC $\Delta P = 4500$ psig

FILM THICKNESS MILS	HELIUM LEAK RATE x 10^9 cc/sec cm^2	HY DROGEN LEAK RATE x 10^9 cc/sec cm^2	OXY GEN LEAK RATE x 10^9 cc/sec cm^2	NITROGEN LEAK RATE x 10^9 cc/sec cm^2	ARGON LEAK RATE x 10^9 cc/sec cm^2	CARBON DIOXIDE LEAK RATE x 10^9 cc/sec cm^2
250	638	172	0.507	0.0063*	0.046	0.084
100	1595	430	3.49	0.0076	0.317	1.27
50	3191	860	8.24	0.0393	1.27	9.51
20	7977	2149	20.6	1.27	4.53	28.5

* 15 YEAR TIME PERIOD

** 20 YEAR TIME PERIOD

INITIAL DISTRIBUTION

1 Naval Research Laboratory, Washington (Code 8000, P. Wilhem)
1 Naval Surface Warfare Center, Dahlgren (Code B05T, L. Triola)
2 United States Air Force Academy, Department of Astronautics, USAF Academy
    CAPT Bettner (1)
    Prof. Humble (1)
1 Kirtland Airforce Base (PL/VT-X, K. Hampsten)
2 Defense Technical Information Center, Alexandria, VA
1 Lawrence Livermore National Laboratory, Livermore, CA (Code L-045, Dr. J. Whitehead)
1 Marshall Space Flight Center, Redstone Arsenal, Huntsville, AL (C. McNeal)
1 Aerojet Inc., Sacramento, CA (W. Yasuhara)
1 Atlantic Research Corp., Gainsville, VA (R. Canny)
1 Beal Aerospace, Dallas, TX (Dr. E. Wernimont)
1 BMDO/TOS, Arlington, VA (J. Kiessling)
1 BMDO/AIT, Arlington, VA (MAJ B. Shipley)
1 Boeing Defense and Space Group, Canoga Park, CA (Dr. H. Lander)
1 Corning Inc., Corning, NY (R. GrosJean)
1 HMX Inc., Mojave, CA (T. Pavia)
1 Lockheed Martin Astronautics, Denver, CO (J. Greenwood)
1 Orbital Sciences Corp., Chandler, AZ (Dr. B. Anderson)
1 School of Aeronautics and Astronautics, West Lafayette, IN (Prof. S. Heister)
1 Ticona Inc., Summit, NJ (Dr. C. McChesney)
1 X-L Laboratories, Grimes, IA (M. Carden)

ON-SITE DISTRIBUTION

4 Code 4BL000D (3 plus Archives copy)
1 Code 473A70D, A. Thompson
1 Code 4731J0D, B. Guest
1 Code 473220D, N. Purcell
1 Code 473230D, M. Minthorn
50 Code 4734E0D, J. Rusek
2 Code 473400D
    E. Saikin (1)
    R. Hoffman (1)
2 Code 473410D
    N. Anderson (1)
    B. Lormand (1)
2 Code 473440D
    P. Cowan (1)
    D. Thompson (1)